Journal of Bionic Engineering (2023) 20:1481–1492
https://doi.org/10.1007/s42235-023-00350-0

RESEARCH ARTICLE

Research on Piezoelectric Driving Microminiature Three-Legged Crawling Robot

Zhongyuan Zheng[1] · Yanru Zhao[1] · Geng Wang[1,2]

Received: 25 September 2022 / Revised: 13 January 2023 / Accepted: 26 January 2023 / Published online: 6 February 2023

Abstract
Micro-robots have the characteristics of small size, light weight and flexible movement. To design a micro three-legged crawling robot with multiple motion directions, a novel driving scheme based on the inverse piezoelectric effect of piezoelectric ceramics was proposed. The three legs of the robot were equipped with piezoelectric bimorphs as drivers, respectively. The motion principles were analyzed and the overall force analysis was carried out with the theoretical mechanics method. The natural frequency, mode shape and amplitude were analyzed with simulation software COMSOL Multiphysics, the optimal size was determined through parametric analysis, and then the micro three-legged crawling robot was manufactured. The effects of different driving voltages, different driving frequencies, different motion bases and different loads on the motion speed of the robot were tested. It is shown that the maximum speed of single-leg driving was 35.41 cm/s, the switching ability between different motion directions was measured, and the movements in six different directions were achieved. It is demonstrated the feasibility of multi-directional motion of the structure. The research may provide a reference for the design and development of miniature piezoelectric three-legged crawling robots.

Keywords Three-legged crawling robot · Piezoelectric drive · Mechanical property analysis · Kinematic features analysis

1 Introduction

Micro-robot is an important research field in robot, which has the characteristics of small size, light weight and flexible movement. The micro-crawling robot has always occupied an important position in many micro-robots because of its certain load capacity, convenient control and high application value. The traditional motor and transmission mechanism makes the robot structure more complex, which will meet many difficulties in the process of miniaturization and assembly [1]. In recent years, the proposed vibration drive system has realized simple structure and encapsulation integration. Piezoelectric ceramics have the advantages of fast response speed, simple structure, small size, power off self-locking, anti-electromagnetic interference and so on. In the vibration drive system, the piezoelectric ceramic is used as the actuator to make the micro-crawling robot, which is convenient for miniaturization research and has good motion performance. Therefore, it is necessary to research the micro-crawling robot driven by the piezoelectric ceramic [2].

In the work on piezoelectric ceramics as actuators, Gao et al. designed an integrated three-legged crawling robot supported by three curved variable-section beams. The whole structure was non-centrosymmetric and made of integrated metal bending. Piezoelectric actuators were arranged on the two driving legs, respectively, and the robot utilized left turn, right turn and forward motion [3]. Zeng et al. proposed a novel piezoelectric ceramic-driven robot. The main body of the robot was manufactured by 3D printing and supported only by the front and back legs. The piezoelectric ceramic was arranged in the center, and the asymmetric friction generated by the spikes on the surface of the legs was used to move forward [4]. Kim et al. designed a millimeter-scale bristle robot with an on-board piezoelectric actuator, which was processed by 3D printing. Bidirectional motion on the millimeter scale was realized by using different driving frequencies [5]. Wu et al. presented a soft robot based on a curved

✉ Yanru Zhao
yanruzhao@163.com

[1] School of Mechanical and Power Engineering, Henan Polytechnic University, Jiaozuo 454000, China

[2] Key Laboratory of Testing Technology for Manufacturing Process of Ministry of Education, Southwest University of Science and Technology, Mianyang 621010, China

unimorph piezoelectric structure. The robot body was made of multiple materials such as piezoelectric ceramics and produces periodic stretching and contraction through piezoelectric effect, thus changing the shape of the robot and producing motion effect [6]. Peng et al. proposed a surface milli-walker based on linear piezoelectric actuation. The robot structure was an integrated design with only two legs, which can walk in a straight line on a plane by fixing piezoelectric ceramics above the structure [7]. Rios et al. designed a hexapod robot machined by a single piezoelectric element. The legs were designed so that the first two modes of resonance overlap and thus produce walking motion while resonating [8]. Li et al. designed a piezoelectric three-legged robot which is actuated by piezoelectric ceramic sheets and supported by three curved beam feet. Piezoelectric ceramics were arranged in the center of the robot structure, and the movement in three directions was realized by utilizing the amplification effect of resonance on vibration deformation and controlling the switching of vibrations between the three legs [9].

With the research of new actuators such as piezoelectric ceramics and the development of new processing methods such as 3D printing, the structure of micro-crawling robots is becoming more and more miniaturized and refined. But as structures get smaller, the robot's locomotion performance suffers. The biped robot can achieve the simplest structural design, but the turning ability is limited. The structure of the multi-legged robot is more complicated than biped robot, and there are higher requirements for leg coordination. Power is also a factor, and the length and weight of wires can influence the robot's movement, and those that can move autonomously without wires tend to be larger and heavier [10].

In this paper, a center-symmetric structure with piezoelectric ceramics arranged on the three legs was designed. The structure design was based on the criteria of simple and easy processing. Applying voltage excitation to different piezoelectric ceramics can act on the three legs respectively. There were three motion directions when driving with one leg and other three motion directions when driving with two legs, which can produce six directions of motion effects with center symmetry. Compared with the existing piezoelectric three-legged crawling robot, the structure has more motion directions, and can quickly switch between different motion directions, improve the motion flexibility, and has a certain load capacity.

2 Structural Design and Mechanical Property Analysis

2.1 Structural Design of the Piezoelectric Robot

A miniature piezoelectric three-legged robot with center symmetry was designed, as shown in Fig. 1. Piezoelectric ceramics were, respectively, arranged on the three legs. The legs and center connectors were processed by 3D printing and pasted with epoxy resin. Piezoelectric ceramics are arranged above and below the legs and the intermediate matrix is a copper alloy material forming a piezoelectric bimorph structure [11]. The length of the piezoelectric bimorph is 35 mm, the width 2.1 mm and thickness 0.72 mm.

The piezoelectric bimorphs are composed of two piezoelectric ceramic sheets and one metal sheet, and the polarization directions of the piezoelectric ceramics above and below are the same. The piezoelectric bimorph will generate reciprocating vibration when piezoelectric ceramics are applied voltage excitation [12].

2.2 The Working Principle of Piezoelectric Ceramic Drive Robot

When the driving voltage frequency of piezoelectric ceramics is near the natural frequency of the legs, the vibration amplitude will increase significantly, and the interaction between the legs and the ground will generate a driving

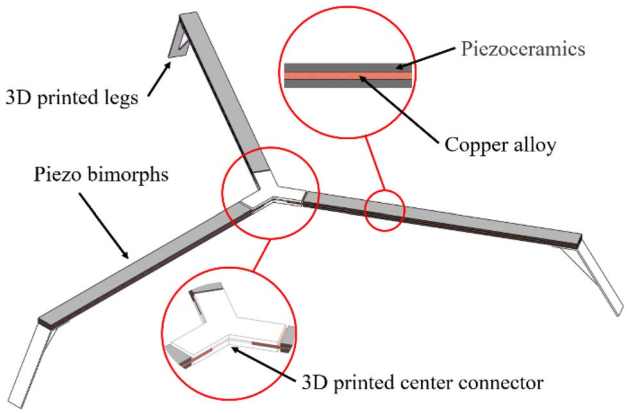

Fig. 1 The miniature piezoelectric three-legged robot

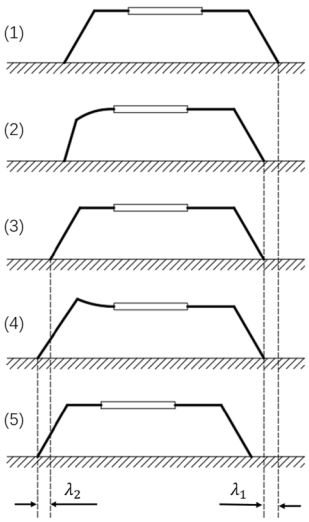

Fig. 2 Movement principle

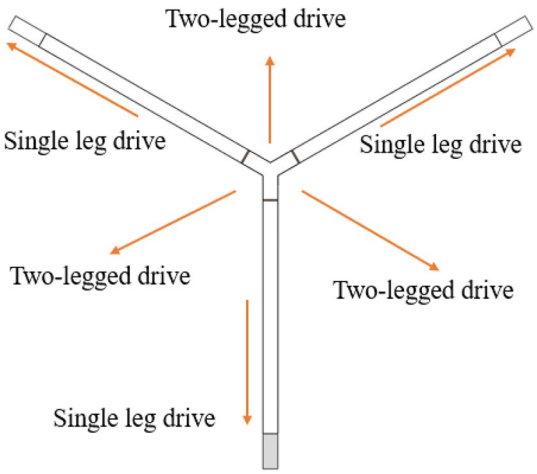

Fig. 3 Movement directions

force to drive the robot forward [13]. The working mode of the piezoelectric ceramic may be selected according to the required vibration effect. The piezoelectric ceramic adopts the d_{31} mode in this paper, in which the direction of the applied voltage and the deformation direction of the piezoelectric sheet are perpendicular to each other [14]. The copper alloy substrate is driven by piezoelectric ceramic to produce periodic bending deformation in this working mode, and the legs connected also produce reciprocating motion [15].

The movement principle and movement direction of piezoelectric ceramic are shown in Fig. 2 and 3, respectively [16]. The boxes are the simplified parts of the piezoelectric bimorph and the thick black lines the simplified parts of the legs.

(1) The robot is in the initial state.

(2) The piezoelectric bimorph is excited by a periodic voltage to bend and the leg bends downward. The pressure of the foot of the motion leg on the ground increases, and its position remains unchanged due to the action of friction [19]. The support leg moves forward by λ_1.

(3) The piezoelectric bimorph is stimulated by the periodic voltage to restore the original state and the foot of the motion leg has a tendency to move upward, so the pressure to the ground decreases. The foot of the motion leg moves forward by λ_1 and the position of the foot of the support leg remains unchanged.

(4) In contrast to step 2, the motion leg bends upward under the excitation of a periodic voltage. The foot of the motion leg has a tendency to move upward and the friction force to the ground decreases, and then the motion leg lifts and moves forward by λ_2. The position of the support leg remains unchanged.

(5) The piezoelectric bimorph returns to its original shape under the excitation of a periodic voltage and the leg bends downward. The pressure of the motion leg to the ground increases and the position remains unchanged. The support leg moves forward by λ_2.

According to the above motion principle, when one leg is driven, the piezoelectric robot will move in the directions of the three legs respectively. The robot will move toward other three directions in the middle of the two legs separately when two legs are driven. So, the robot has a total of six motion directions.

2.3 Mechanical Properties Analysis of Piezoelectric Robot

According to the working principle, the piezoelectric bimorph deforms by the excitation of voltage, and when the frequency is close to the natural frequency of the leg, it will cause resonance and the amplitude will increase. When the robot's legs interact with the ground, they are affected by the support force and friction force, and the amplitude and friction force affect the movement speed of the robot. Therefore, it is necessary to analyze the deformation of the piezoelectric bimorph, the fundamental frequency and the force of the robot during motion. Stress T_i and strain S_i are often used to represent the mechanical properties of piezoelectric ceramics. When Hooke's law is satisfied, the linear relationship between the stress and strain experienced by an elastic body in its elastic range satisfies can be expressed as follows [17]:

$$S_i = \sum_{j=1}^{6} s_{ij} T_j = s_{ij} T_j \quad i, j = 1, 2, 3, \cdots, 6, \tag{1}$$

$$T_i = \sum_{j=1}^{6} c_{ij} S_j = c_{ij} S_j \quad i,j = 1,2,3,\cdots,6, \tag{2}$$

where s_{ij} is the elastic compliance coefficient of the piezoelectric ceramic material, $s_{ij}=s_{ji}$; c_{ij} is the elastic stiffness coefficient of the piezoelectric ceramic material, $c_{ij}=c_{ji}$. The relationship between s_{ij} and c_{ij} may be computed below.

$$s_{ij} = \left(c_{ij}\right)^{-1}. \tag{3}$$

Piezoelectric bimorph can be deemed as a three-layer beam element. Make the following assumptions: (1) the influence of the adhesive layer between the piezoelectric ceramic and the substrate is ignored; (2) the piezoelectric bimorph is only loaded at the end of the actuation zone along the thickness direction and has no axial load; (3) the effect of the temperature gradient between the piezoelectric ceramic and the substrate is negligible. According to the above assumptions, the matrix strain ε and matrix curvature κ are related to the force N and moment M as follows [18]:

$$\begin{bmatrix} N \\ M \end{bmatrix} = \begin{bmatrix} A_{ij} & B_{ij} \\ B_{ij} & D_{ij} \end{bmatrix} \begin{bmatrix} \varepsilon \\ \kappa \end{bmatrix}, \tag{4}$$

where the formulas for matrices A, B and D are as follows:

$$A_{ij} = \Sigma_n \left(\overline{Q_{ij}}\right)_n \left(z_n - z_{n-1}\right), \tag{5}$$

$$B_{ij} = \frac{1}{2}\Sigma_n \left(\overline{Q_{ij}}\right)_n \left(z_n^2 - z_{n-1}^2\right), \tag{6}$$

$$D_{ij} = \frac{1}{3}\Sigma_n \left(\overline{Q_{ij}}\right)_n \left(z_n^3 - z_{n-1}^3\right), \tag{7}$$

where N and M are the forces and moments sustained on the unit width of the piezoelectric bimorph, respectively; Q is the stiffness matrix of the laminate; κ is the neutral plane curvature of the laminate; ε is the neutral surface strain of the laminate; n denotes the number of layers; Z_n denotes the thickness of the nth layer. According to the above formula, the relationship between the stress and strain of the piezoelectric bimorph can be obtained as follows:

$$\begin{bmatrix} \varepsilon_x \\ \varepsilon_y \\ \varepsilon_{xy} \\ \kappa_x \\ \kappa_y \\ \kappa_{xy} \end{bmatrix} = C\left(\begin{bmatrix} 0 \\ 0 \\ 0 \\ M_x(x) \\ 0 \\ 0 \end{bmatrix} + \begin{bmatrix} N_x^p \\ N_y^p \\ 0 \\ M_x^p \\ M_y^p \\ 0 \end{bmatrix}\right), \tag{8}$$

$$C = \begin{bmatrix} A_{ij} & B_{ij} \\ B_{ij} & D_{ij} \end{bmatrix}^{-1}, \tag{9}$$

where N^P and M^P, respectively, represent the internal force and torque generated by the inverse piezoelectric effect after applying voltage excitation; $M_x(x)$ represents the moment per unit width at a distance x from the surface of the piezoelectric bimorph.

Equation (10) represents the constitutive relationship between the applied electric field E and the output displacement δ of the tip of the actuation region; Eq. (11) is the relationship between the applied electric field E and the output force F; Eq. (12) is the fundamental frequency [19].

$$\delta = \frac{3L^2}{2t} \frac{(1+B)(1+2B)}{AB^3 + 3B^2 + 3B + 1} d_{31} E, \tag{10}$$

$$F = \frac{3wt^2 E_p}{8L} \frac{2B+1}{(B+1)^2} d_{31} E, \tag{11}$$

$$\omega_n = \frac{\lambda_i h}{4\pi L} \sqrt{\frac{E_p}{\rho_p}} \left[\frac{1 + 3(1+2B)^2 + 4AB^3}{4(1+B)^2(BC+1)}\right]^{1/2}, \tag{12}$$

where δ is the static displacement; d_{31} is the piezoelectric constant; w is the beam width; L is the beam length. $A=E_m/E_p$, $B=t_m/2t_p$, $C=\rho_m/\rho_p$, $t=t_m+2t_p$. E_m, t_m, ρ_m and E_p, t_p, ρ_p represent the Young's modulus, thickness and density of the substrate and piezoelectric layer, respectively. E represents the electric field strength applied to the thickness direction of the piezoelectric ceramic, $E=V/t_p$.

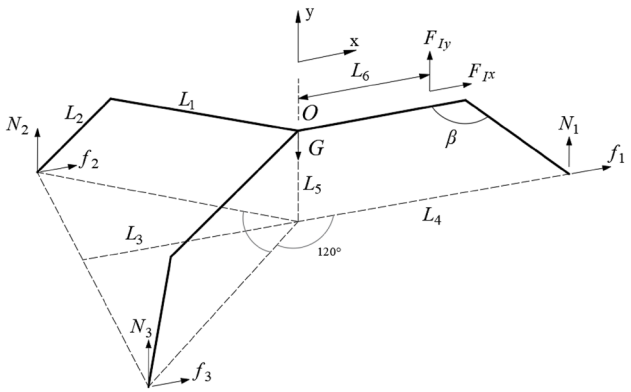

Fig. 4 Overall force of the piezoelectric three-legged robot

The overall force analysis of the piezoelectric three-legged robot is shown in Fig. 4. The black bold font is the simplified part of the robot structure. The leg applied voltage is marked as the motion leg, numbered 1, and the remaining two legs are recorded as support legs, numbered 2 and 3.

In Fig. 4, F_I is the inertial force generated by the motion leg of the piezoelectric bimorph; N_1 and f_1 are the support force and friction force bore of the motion leg on the ground; N_2 and f_2 are the support force and friction force bore of the support legs on the ground; G is the gravity of the robot; L_1 is the length of the piezoelectric bimorph; L_2 is the length of the legs; L_3 is the length from the center of the robot to the support legs; L_4 is the length from the center of the robot to the motion leg; L_5 is the height of the robot.

The motion leg deforms and bends downward, increasing the pressure on the ground. The support force and friction force of the motion leg become larger, and the robot moves forward under the action of the friction force. Suppose that the support force and friction force are the same on both support legs, that is, $N_2=N_3$, $f_2=f_3$, then the balance conditions of the overall force system of the robot may be computed as follows:

$$f_1 + 2f_2 + F_{I_x} = 0, \tag{13}$$

$$N_1 + 2N_2 + F_{I_y} - G = 0, \tag{14}$$

$$F_{I_y}L_6 + N_1L_4 + \left(f_1 + 2f_2\right)L_5 - 2N_2L_3 = 0. \tag{15}$$

From Eqs. (13)–(15), the support forces and friction forces may be obtained, namely:

$$N_1 = \frac{GL_3 + F_{I_x}L_5 - F_{I_y}\left(L_3 + L_6\right)}{L_3 + L_4}, \tag{16}$$

$$N_2 = \frac{GL_4 - F_{I_x}L_5 + F_{I_y}\left(L_6 - L_4\right)}{2\left(L_3 + L_4\right)}, \tag{17}$$

$$f_1 = \mu N_1, \tag{18}$$

$$f_2 = \mu N_2. \tag{19}$$

The formulas describe the relationship between the support force and the friction force among the three legs when the robot moves. The friction of the motion leg drives the robot forward, the friction of the support legs hinders the movement, and the magnitude of the friction affects the speed of the robot. When the vibration frequency of the piezoelectric bimorph of the motion leg is close to the natural frequency, the amplitude increases and the moving speed increases.

3 Simulation Analysis

3.1 Boundary Condition Setting and Overall Deformation Analysis

The 3D model of the robot was built using Solidworks, and then imported into COMSOL Multiphysics for simulation analysis. The copper alloy was selected as piezoelectric bimorph substrate, the material 850 in PZT-8 series as piezoelectric ceramic, the resin material 9400 was adopted for the 3D printing parts, and the detailed free tetrahedral mesh was used [20]. A potential boundary condition of 155 V voltage was added to the upper layer of the bimorph and a ground boundary condition to the lower layer. The overall deformation simulation result of the piezoelectric robot is shown in Fig. 5, and the black thin line represents the initial state.

The piezoelectric bimorph of the motion leg bent and deformed in the vertical direction, which drove the movement of the leg, and the deformation of the support leg was small. This deformation was the same as that described in Sect. 2.2.

3.2 Modal Analysis

The eigenfrequency simulation analyses of the legs were performed to obtain the vibrational modes. The finite element calculation results of the first- to sixth-order vibrational modes are shown in Fig. 6. The black thin line is the initial state [21].

The vibrational modes were selected according to the situation and motion principle of the first- to sixth-order vibrational modes [22]. The legs of the first-order vibrational modes reciprocate vertically, and the legs of the second-order, fifth-order and sixth-order modes mainly vibrate laterally. The legs of the third-order and fourth-order modes

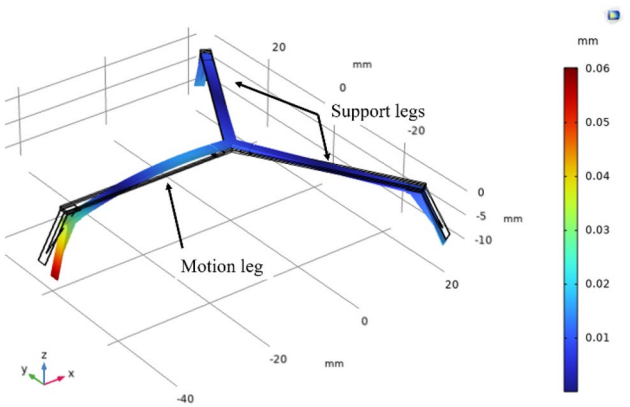

Fig. 5 Overall deformation of the piezoelectric robot

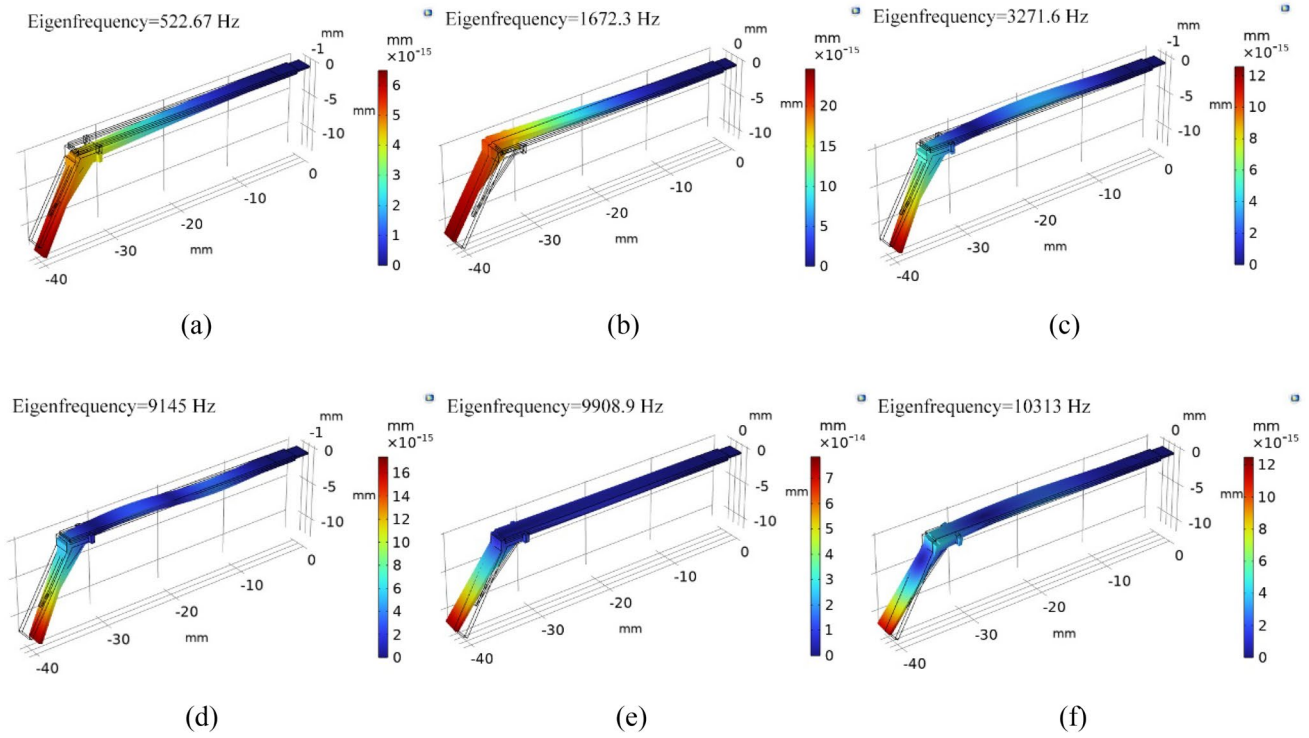

Fig. 6 The first- to sixth-order vibrational modes. **a** The first-order vibrational mode. **b** The second order. **c** The third order. **d** The fourth-order. **e** The fifth order. **f** The sixth order

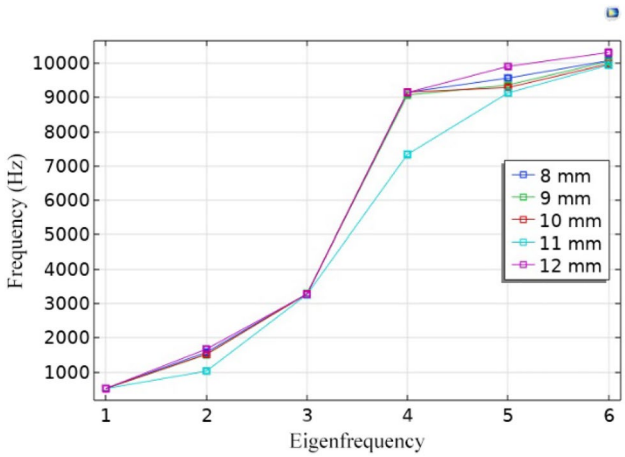

Fig. 7 Leg lengths and natural frequency

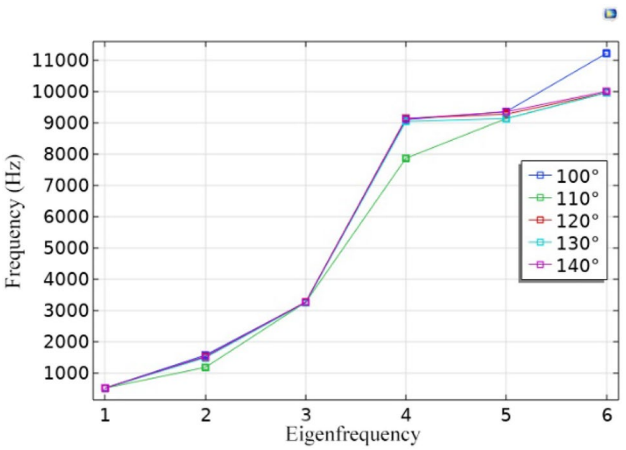

Fig. 8 Leg angles and natural frequency

vibrate vertically, but the deformation of the piezoelectric bimorph is large, which will affect the service life. In the motion principle above, the motion leg vibrate vertically, which is similar to the vibration of the first-order mode, so the first-order mode is selected, and the frequency is 522.67 Hz [23].

According to the parametric analysis of the leg structure, the influence of the change of the lengths and angles of the legs on the natural frequency of the structure can be obtained [24]. Figure 7 shows the frequencies of the first six-order modes obtained from the parametric scanning of the leg lengths and Fig. 8 shows the results of parametric scanning of the angles among the legs and the piezoelectric bimorph. It was demonstrated that the change in leg lengths and angles has little effect on the first-order eigenfrequency, and the difference expands from the second-order onward.

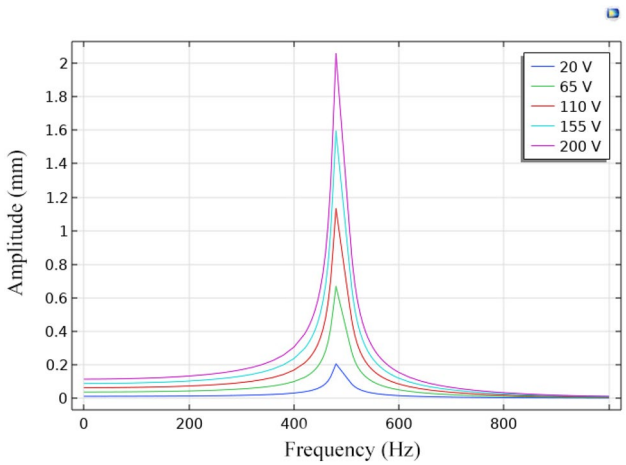

Fig. 9 Frequency domain analysis

The eigenfrequency analysis can only obtain vibrational modes and frequency information, so the amplitude obtained in the eigenfrequency analysis is inaccurate. After analyzing the eigenfrequencies to obtain the vibrational modes, the structure was analyzed in the frequency domain to obtain the vibration amplitude.

3.3 Parametric Sweep Analysis

The driving voltage of the motion leg was parameterized and analyzed in the frequency domain, as shown in Fig. 9. It was indicated that the amplitude increased significantly around 500 Hz, which is near the first-order natural frequency of the leg. The amplitude decreased away from 500 Hz, but increased with the driving voltage [25]. The amplitude affects the movement speed of the robot. It should be shown in the experiment that the speed of the robot increases significantly when the driving voltage frequency is around 500 Hz, and the speed increases with the increase of the voltage.

The effect of changes in leg lengths and angles among the legs and the piezoelectric bimorphs on the magnitude of the first-order natural frequency is shown in Fig. 10. It was shown that the first-order natural frequency of the leg fluctuated around 522 Hz after changing the two parameters. The natural frequency decreased when the angle is less than 110° and the length less than 9 mm.

The effect of leg lengths and angles among the legs and the piezoelectric bimorphs on the maximum amplitude is shown in Fig. 11. It was found that the longer the leg length is, the larger the amplitude will be, and the amplitude increases in a fluctuation pattern with the angles. The maximum amplitude increases before leg angles reaching 120°, decreases from 120° to 130°, and, then increases approaching 140°.

When the frequency of the driving voltage is near the natural frequency of the leg, the amplitude will increase, so the frequency of the driving voltage in the experiment refers to the frequency obtained by the simulation. It was found from the simulation results that the change of leg structure has little effect on the first-order natural frequency. The magnitude of the amplitude affects the movement speed of the robot. The increase of the angle among the legs and the piezoelectric bimorphs causes the amplitude to increase in a fluctuation pattern, and the increase of the leg length amplifies the amplitude. According to the above simulation results, the sizes of the piezoelectric robot were determined, as shown in Table 1.

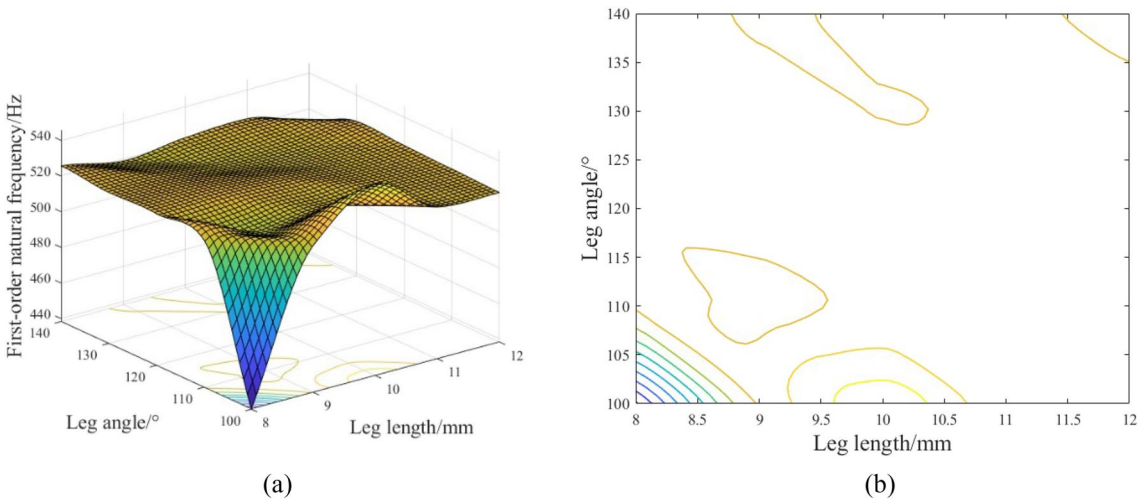

(a) (b)

Fig. 10 Parametric scanning of leg lengths and angles. **a** Leg lengths and angles; **b** contour map

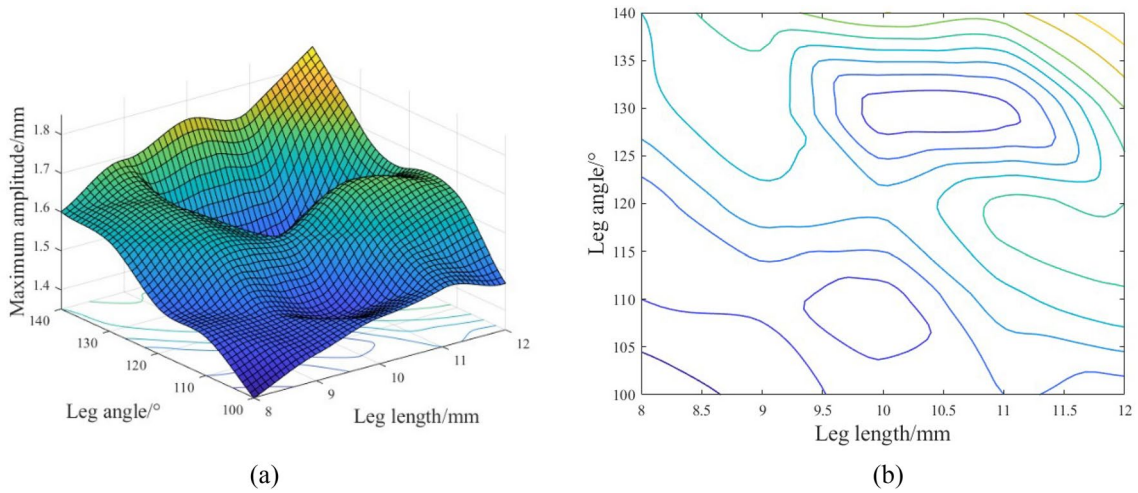

Fig. 11 Influence of leg lengths and angles on amplitude. **a** Leg length and angle; **b** contour map

Table 1 Parameters of the piezoelectric robot

Parameters	Values
Leg length	10 mm
Leg width	2.1 mm
Leg thickness	0.5 mm
Angles among the legs and the piezoelectric bimorphs	120°
Piezoelectric bimorph length	35 mm
Piezoelectric bimorph width	2.1 mm
Piezoelectric bimorph thickness	0.72 mm
Overall length of the robot	78 mm
Overall width of the robot	42 mm
Overall height of the robot	10 mm
Robot weight	1.203 g

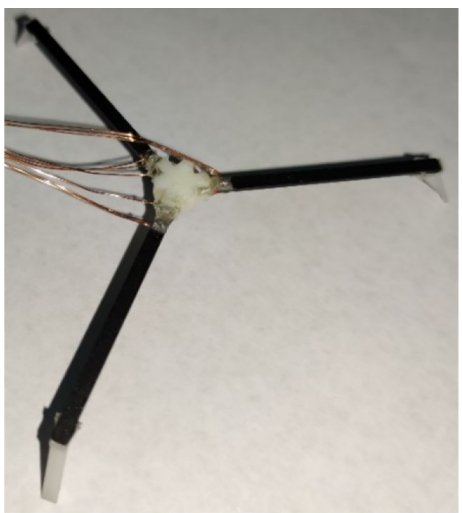

Fig. 12 Robot prototype

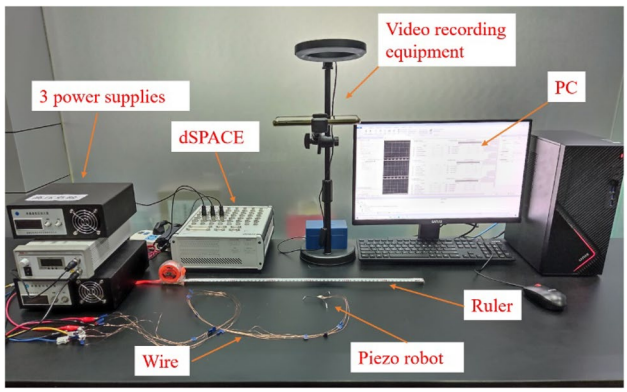

Fig. 13 Experiment equipment

4 Experimental Results

The piezoelectric robot prototype is shown in Fig. 12, and the experimental equipment is shown in Fig. 13. A control signal framework was built in Simulink and imported into dSPACE for signal processing. The control signal was observed and changed on the computer, the command processed through dSPACE and sent to the voltage amplifier for amplifying, and, then transmitted to the robot through the wire. A video recording device was fixed above the robot to record the movement of the robot and sent to the PC for processing. A ruler was placed next to the robot to measure the distance during the test.

The driving voltage was divided into four groups from 20 to 155 V, and multiple groups of movement conditions of the robot within different driving frequencies from 45 to 825 Hz were tested. The single-leg driving, double-leg driving, different motion bases and motion speeds under

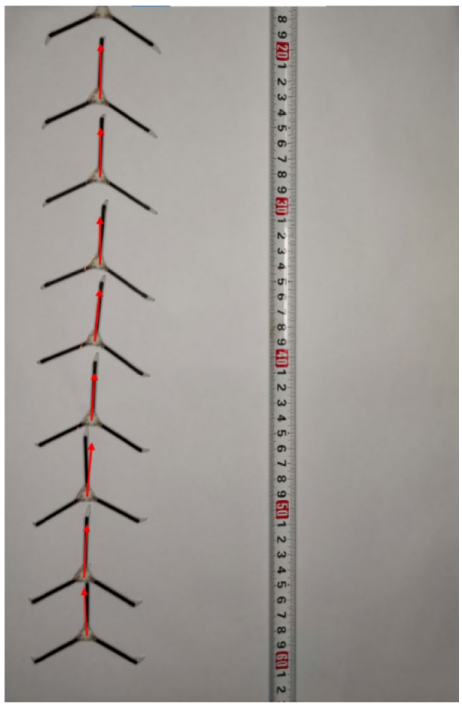

Fig. 14 Single-leg driving

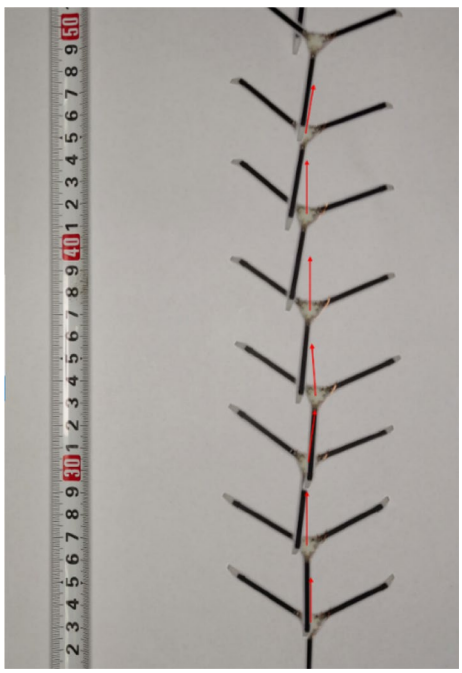

Fig. 15 Double-leg driving

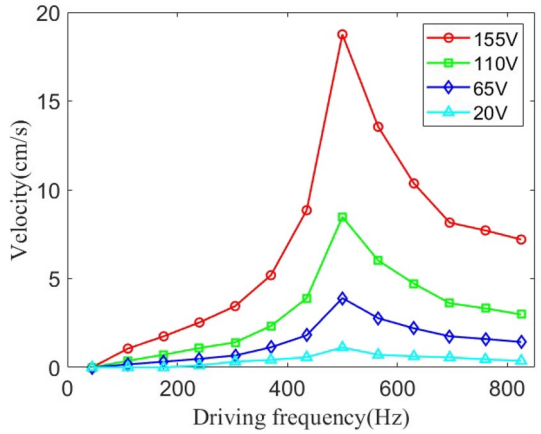

Fig. 16 Single-leg driving on A0 paper

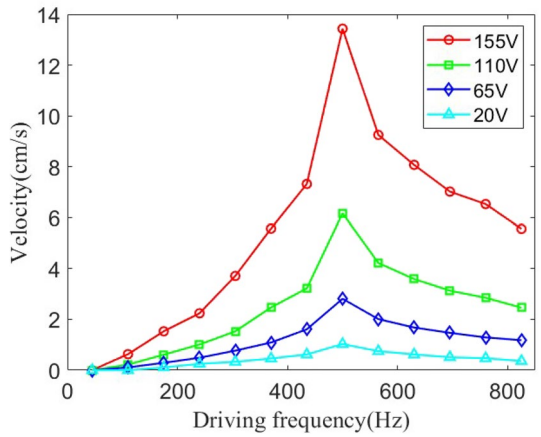

Fig. 17 Double-leg driving on A0 paper

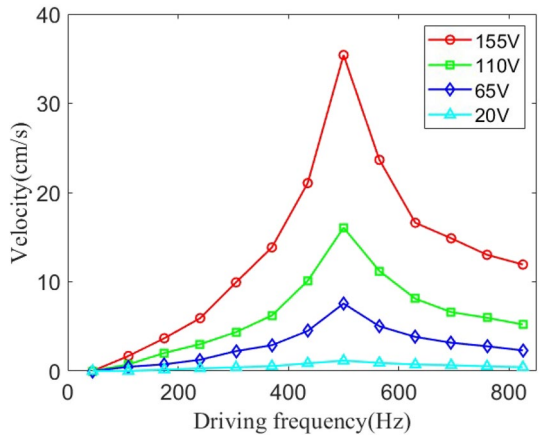

Fig. 18 Single-leg driving on desktop

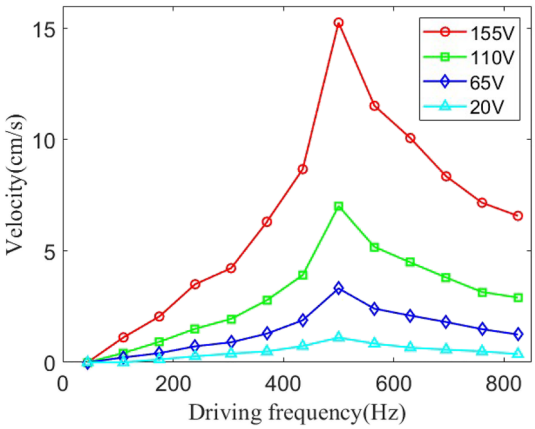

Fig. 19 Double-leg driving on desktop

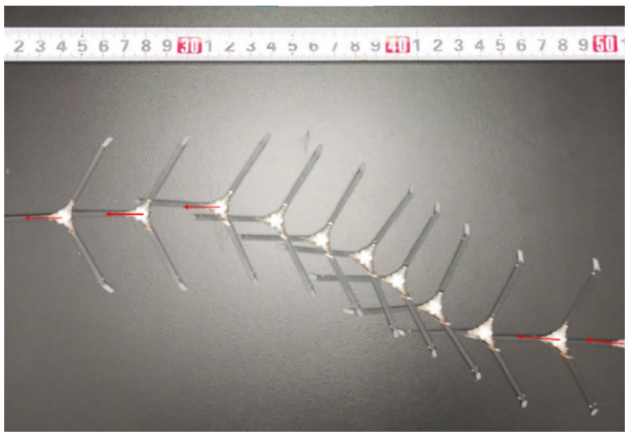

Fig. 20 Movement directions switching test

different loads were measured. The motions of single-leg driving and double-leg driving are shown in Figs. 14 and 15, respectively. It was shown that the straightness was fine by single-leg driving and the movement route was offset by double-leg driving due to the machining error and the friction force of the two moving legs cannot be exactly the same.

The movement speeds of single-leg driving and double-leg driving on the A0 paper were examined, as shown in Figs. 16 and 17, respectively. It was found that the peak of movement velocity appeared when the driving voltage frequency was near the first resonant frequency of the leg. When the driving voltage frequency was lower than 500 Hz, the motion speed decreased sharply, and when the driving frequency was higher than 500 Hz, the speed also decreased, but the degree of decrease was relatively small. At 500 Hz driving voltage frequency, the single-leg driving speed was 18.75 cm/s and double-leg driving speed was 13.43 cm/s.

To study the effect of different moving surfaces on the speed, the robot was tested again on a table, as shown in Figs. 18, 19. It was found that when moving on different surfaces, the robot has different maximum moving speed, but within the same frequency range. The maximum speed of single-leg driving on the desktop is 35.41 cm/s and that of double-leg driving is 15.26 cm/s. The reason for the analysis is that the friction among the A0 paper and the robot's legs is smaller than that of the table surface, and if the friction is too small, the robot will slip. The surface of the table used in the experiment has regular lines and the roughness is relatively uniform. The difference in roughness among the three legs will also affect the motion of the robot.

Compared with the simulation results, when the driving frequency is close to 500 Hz, it is located near the first-order natural frequency of the leg. Resonance causes the amplitude of the leg to increase significantly and the amplitude increases with the increase of the voltage and affects the movement speed of the robot. It is illustrated in the experiment that when the driving frequency is around 500 Hz, the speed of the robot running on different surfaces increases significantly, and the speed increases with the increase of the voltage. It is consistent with the analysis of the motion principle in Sect. 2 and the simulation data are the same, which also proves the correctness of the motion principle and simulation data.

To detect the robot's ability to switch among different motion directions, the switching between single-leg driving and double-leg driving was tested on the table surface. As shown in Fig. 20, the robot can realize the conversion among different motion directions by switching between single-leg driving and double-leg driving. A small tray 0.844 g was fixed in the center of the robot, and then standard weight was placed in the tray to test the speed of the robot under load. As the load increased, the speed of the robot decreased drastically, as shown in Fig. 21.

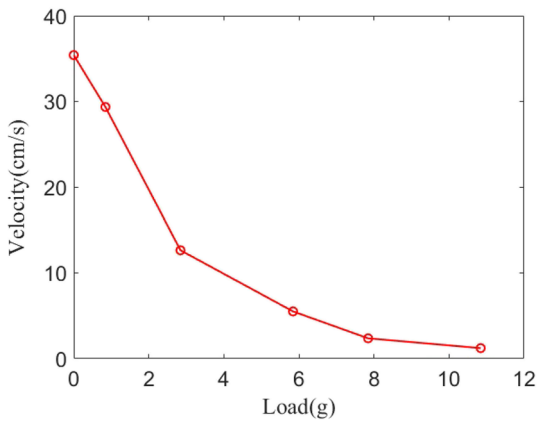

Fig. 21 Load experiment

It was demonstrated that the speed of single-leg motion of the piezoelectric robot is faster than that of the double-leg motion, and the motion is relatively stable on a plane with relatively uniform roughness. The robot can switch among six centrosymmetric motion directions.

5 Conclusions

A microminiature piezoelectric three-legged robot with overall centrosymmetric structure was designed and the following conclusions may be obtained by simulation and experimental verification.

(1) The motion principle and mechanical properties of the robot were analyzed by theoretical mechanics method.
(2) The influence of different structural parameters of the robot on the key parameters of motion was obtained through simulation calculation, and the structural size of the piezoelectric robot was determined, and, then a prototype was processed.
(3) When the driving voltage frequency is near the first-order natural frequency of the leg, the movement speed of the robot increases significantly. The movement speed of the robot varies greatly on surfaces with different roughness and has a large influence by the load bearing. The robot can achieve center-symmetric movements in six different directions, and has more flexible movement capabilities than the existing miniature three-legged crawling robots. Based on this, it is further optimized for use in tiny gaps or other tiny places. In practical application, the load may be replaced with micro sensors, micro cameras, etc., so the robot has potential application value in environmental detection, biomedicine and so on.

Supplementary Information The online version contains supplementary material available at https://doi.org/10.1007/s42235-023-00350-0.

Acknowledgements This work was supported by the National Natural Science Foundation of China (grant no. 51505133), by Key Research Project in Colleges and Universities of Henan Province (23A460010), by Opening Project of Henan Engineering Laboratory of Photoelectric Sensor and Intelligent Measurement and Control, Henan Polytechnic University (grant no. HELPSIMC-2020-006).

Data Availability Data sharing is not applicable to this article, as no datasets were generated or analyzed during the current study.

Declarations

Conflict of Interest The authors declare that they have no conflict of interest.

References

1. Hariri, H., Bernard, Y., & Razek, A. (2018). 2-D traveling wave driven piezoelectric plate robot for planar motion. *IEEE/ASME Transactions on Mechatronics, 23*(1), 242–251.
2. Lee, G., You, K., Kang, T., Yoon, K. J., Lee, J. O., & Park, J. K. (2010). Modeling and design of h-infinity controller for piezoelectric actuator LIPCA. *Journal of Bionic Engineering, 7*(2), 168–174.
3. Gao, Y. F., & Zhou, S. X. (2021). A piezoelectric-driven three-legged crawling robot. *Chinese Journal of Theoretical and Applied Mechanics, 53*(12), 3354–3365.
4. Zeng, X. L., Wu, Y., Han, S. Y., Liu, Y. B., Xiu, H. H., Tian, F. J., & Ren, L. Q. (2021). Theoretical and experimental investigations into a crawling robot propelled by piezoelectric material. *Micromachines, 12*(12), 1577.
5. Kim, D., Hao, Z., Mohazab, A. R., & Ansari, A. (2020). On the forward and backward motion of milli-bristlebots. *International Journal of Non-Linear Mechanics, 127*, 103551.
6. Wu, Y. C., Yim, J. K., Liang, J. M., Shao, Z. C., Qi, M. J., Zhong, J. W., Luo, Z. H., Yan, X. J., Zhang, M., Wang, X. H., Fearing, R. S., Full, R. J., & Lin, L. W. (2019). Insect-scale fast moving and ultrarobust soft robot. *Science Robotics., 4*(32), 1594.
7. Peng, H. M., Yang, J. Z., Lu, X. L., Zhu, P. C., & Wu, D. W. (2018). A lightweight surface milli-walker based on piezoelectric actuation. *IEEE Transactions on Industrial Electronics, 66*(10), 7852–7860.
8. Rios, S. A., Fleming, A. J., & Yong, Y. K. (2018). Monolithic piezoelectric insect with resonance walking. *IEEE/ASME Transactions on Mechatronics, 23*(2), 524–530.
9. Li, K., & Xu, J. (2015). Plane motion of a tripod robot driven by piezoelectric resonance. *Journal of Dynamics and Control, 13*(6), 454–461.
10. Du, Z. W., Fang, H. B., Zhan, X., & Xu, J. (2018). Experiments on vibration-driven stick-slip locomotion: A sliding bifurcation perspective. *Mechanical Systems and Signal Processing, 105*, 261–275.
11. Goldberg, B., Zufferey, R., Doshi, N., Helbling, E. F., Whittredge, G., Kovac, M., & Wood, R. J. (2018). Power and control autonomy for high-speed locomotion with an insect-scale legged robot. *IEEE Robotics and Automation Letters, 3*(2), 987–993.
12. Cheon, S. K., Park, M. H., Jeong, S. S., Jun, H. I., Kim, T. H., & Park, T. G. (2019). Development of small robot using piezoelectric benders. *Integrated Ferroelectrics, 195*(1), 81–90.
13. Su, Q., Quan, Q. Q., Deng, J., & Yu, H. P. (2018). A quadruped micro-robot based on piezoelectric driving. *Sensors, 18*(3), 810.
14. Hernando-García, J., García-Caraballo, J. L., Ruiz-Díez, V., & Sánchez-Rojas, J. L. (2021). Comparative study of traveling

and standing wave-based locomotion of legged bidirectional miniature piezoelectric robots. *Micromachines, 12*(2), 171.
15. Hernando-García, J., García-Caraballo, J. L., Ruiz-Díez, V., & Sánchez-Rojas, J. L. (2020). Motion of a legged bidirectional miniature piezoelectric robot based on traveling wave generation. *Micromachines, 11*(3), 321.
16. Zhou, J. T., Suzuki, M., Takahashi, R., Tanabe, K., Nishiyama, Y., Sugiuchi, H., Maeda, Y., & Fuchiwaki, O. (2020). Development of a Δ-type mobile robot driven by three standing-wave-type piezoelectric ultrasonic motors. *IEEE Robotics and Automation Letters, 5*(4), 6717–6723.
17. Peng, H. M., Mao, T., & Lu, X. L. (2020). A small legged deformable robot with multi-mode motion. *Journal of Intelligent Material Systems and Structures, 31*(5), 704–718.
18. Park, T., & Cha, Y. (2019). Soft mobile robot inspired by animal-like running motion. *Scientific Reports, 9*(1), 1–9.
19. Mao, T., Peng, H. M., Lu, X. L., & Zhao, C. S. (2019). A small locust inspired actuator driven by shape memory alloys and piezoelectric strips. *Smart Materials and Structures, 28*(10), 105051.
20. Fang, H. B., & Wang, K. W. (2017). Piezoelectric vibration-driven locomotion systems–exploiting resonance and bistable dynamics. *Journal of Sound and Vibration, 391*, 153–169.
21. Rios, S. A., Fleming, A. J., & Yong, Y. K. (2016). Miniature resonant ambulatory robot. *IEEE Robotics and Automation Letters, 2*(1), 337–343.
22. Jalili, H., Salarieh, H., & Vossoughi, G. (2017). Study of a piezo-electric actuated vibratory micro-robot in stick-slip mode and investigating the design parameters. *Nonlinear Dynamics, 89*(3), 1927–1948.
23. Hariri, H. H., Soh, G. S., Foong, S., & Wood, K. (2017). Locomotion study of a standing wave driven piezoelectric miniature robot for bi-directional motion. *IEEE Transactions on Robotics, 33*(3), 742–747.
24. Jalili, H., Vossoughi, G., & Salarieh, H. (2016). Motion analysis of a vibrational microrobot with two perpendicular harmonic actuators and deriving the design parameters in stick–slip mode. *Journal of Computational and Nonlinear Dynamics, 11*(2), 021003.
25. Hariri, H., Bernard, Y., & Razek, A. (2015). Dual piezoelectric beam robot: The effect of piezoelectric patches' positions. *Journal of Intelligent Material Systems and Structures, 26*(18), 2577–2590.